UNCERTAINTIES IN SPHERICAL NEAR-FIELD ANTENNA MEASUREMENTS[1]

Michael H. Francis and Ronald C. Wittmann
National Institute of Standards and Technology, Boulder, CO 80305
francis@boulder.nist.gov, wittmann@boulder.nist.gov

Jin-Seob Kang
Korean Research Institute of Standards and Science, Daejeon 305-600, Korea
jinskang@kriss.re.kr

Abstract. A general approach is presented for estimating uncertainties in far-field parameters obtained from spherical near-field antenna measurements. The error is approximately bounded in terms of the uncertainty of the probe's receiving pattern and the uncertainty in the near-field coupling over the mutually subtended solid angle. We give some specific examples, including a discussion on estimating uncertainty due to multiple reflections between probe and test antenna.

1. Introduction.

Uncertainty analysis for spherical near-field measurements is an on-going topic of research [1], [2], [3], [4]. Previous work has relied heavily on simulation studies; however, we seek a more analytic approach following [5] and [6].

In near- to far-field transformation, the far-field error in a given direction depends on errors in near-field measurements over a surface and in the receiving pattern of the probe. In contrast, error in a far-field measurement depends only on measurement errors in the direction of interest and in the on-axis gain and polarization of the probe. In this discussion we consider the nonlocal propagation of uncertainty in near-field spherical scanning. Our formulation reduces to a direction-by-direction analysis as the separation of probe and test antenna increases.

2. Near-Field Spherical Scanning Summarized.

Here we present a brief synopsis of near-field spherical scanning theory. A complete discussion may be found in [1].

The far-field radiation of an antenna can be characterized by

$$\mathbf{E}(\mathbf{r}) \underset{r\to\infty}{\sim} \mathbf{t}(\hat{\mathbf{r}}) \frac{\exp(ikr)}{ikr} a_0. \tag{1}$$

This formula embodies the linear relationship between the radiated electric field $\mathbf{E}(\mathbf{r})$ and the excitation a_0. The transmission function $\mathbf{t}(\hat{\mathbf{r}})$ may be expanded as

$$\mathbf{t}(\hat{\mathbf{r}}) = \sum_{n=1}^{N} \sum_{m=-n}^{n} \left[t_{nm}^{1} \mathbf{X}_{nm}(\hat{\mathbf{r}}) + t_{nm}^{2} \mathbf{Y}_{nm}(\hat{\mathbf{r}}) \right], \tag{2}$$

where $\mathbf{X}_{nm}$ and $\mathbf{Y}_{nm} = i\hat{\mathbf{r}} \times \mathbf{X}_{nm}$ are vector spherical harmonics [7, chapter 16], which depend only on direction, and t_{nm}^{ℓ} are (unknown) modal coefficients.

In near-field spherical scanning, the antenna under test (AUT) is characterized by measurement with a probe that moves over a spherical surface enclosing the AUT. The response of the probe depends on the measurement radius r, the position specified by the spherical coordinate angles θ and φ, and the rotation angle χ about the probe axis. To simplify the collection and processing of measurement data, we follow common practice [1] and restrict our attention to special $\mu = \pm 1$ probes. For these probes, we can define a measurement vector that also may be expanded in spherical harmonics:

$$\mathbf{w}(\mathbf{r}) = \sum_{nm}^{N} \left[T_{nm}^{1}(r) \mathbf{X}_{nm}(\hat{\mathbf{r}}) + T_{nm}^{2}(r) \mathbf{Y}_{nm}(\hat{\mathbf{r}}) \right]. \tag{3}$$

The summation, which has the same limits as in (2), is written in abbreviated form here and below. Determination of $\mathbf{w}(\mathbf{r})$ requires two measurements at each probe location, which is reasonable in view

[1] U.S. Government contribution not subject to copyright in the United States.

ISBN: 89-86522-77-2 94460©KEES

of the polarization of electromagnetic fields. The relationship between the (known) T^{ℓ}_{nm} and the t^{ℓ}_{nm} is given by the probe-correction equations

$$\begin{pmatrix} T^1_{nm} \\ \\ T^2_{nm} \end{pmatrix} = \mathbf{M}_n \begin{pmatrix} t^1_{nm} \\ \\ t^2_{nm} \end{pmatrix}. \tag{4}$$

Matrices $\mathbf{M}_n$ are functions of $\mathbf{s}$, the known receiving function of the probe.

3. RMS Uncertainties in Near-Field Measurements.

According to [8], the uncertainty in the calculated transmission function is

$$u_t^2 (\hat{\mathbf{r}}) = \alpha^2 u_w^2 (\mathbf{r}) + \tau^2 \beta^2 \|\mathbf{t}\|^2_{\Omega(\hat{\mathbf{r}})} u_s^2 (\hat{\mathbf{z}}) \tag{5}$$

with

$$\tau^2 = 2. \tag{6}$$

The norm $\|\mathbf{f}\|_{\Omega(\mathbf{r})}$ is the root mean square (RMS) value of $\mathbf{f}(r\hat{\mathbf{r}}')$ over the solid angle $\Omega(\mathbf{r})$:

$$\|\mathbf{f}\|^2_{\Omega(\mathbf{r})} = \frac{1}{\Omega(\mathbf{r})} \int_{\Omega(\mathbf{r})} \|\mathbf{f}(\mathbf{r}')\|^2 \, d\hat{\mathbf{r}}'. \tag{7}$$

Following Yaghjian [9], we assume that the probe and test antenna interact mainly through the mutually subtended "sheaf of angles" $\Omega(\mathbf{r})$ (see Figure 1). The uncertainties in (5) are to be interpreted as bounds for RMS errors in $\mathbf{w}$, $\mathbf{s}$ and $\mathbf{t}$; that is,

$$u_w(\mathbf{r}) \gtrapprox \|\delta\mathbf{w}\|_{\Omega(\mathbf{r})}, \quad u_s(\hat{\mathbf{z}}) \gtrapprox \|\delta\mathbf{s}\|_{\Omega(\hat{\mathbf{z}})}, \quad u_t(\hat{\mathbf{r}}) \gtrapprox \|\delta\mathbf{t}\|_{\Omega(\hat{\mathbf{r}})}. \tag{8}$$

Finally,

$$\alpha(r) \equiv \max_{1\le n\le N} \left\|\mathbf{M}_n^{-1}\right\|_2, \tag{9}$$

and β is either β_1 or β_2:

$$\beta_1(r) \equiv \frac{2\pi}{\|\mathbf{t}\|_{4\pi}} \sqrt{\frac{1}{4\pi} \sum_{nm}^{N} \xi_n^2 \left\|\mathbf{M}_n^{-1}\right\|_2^2 \left(\left|t^1_{nm}\right|^2 + \left|t^2_{nm}\right|^2\right)} \tag{10}$$

$$\beta_2(r) \equiv 2\pi \max_{1\le n\le N} \left(\xi_n \left\|\mathbf{M}_n^{-1}\right\|_2\right), \qquad \beta_1 \le \beta_2. \tag{11}$$

Formulas for $\mathbf{M}_n$ and ξ_n are given in [8, equations (5) and (59)]. Equations 10-11 are improvements over the estimate for β found in [8].

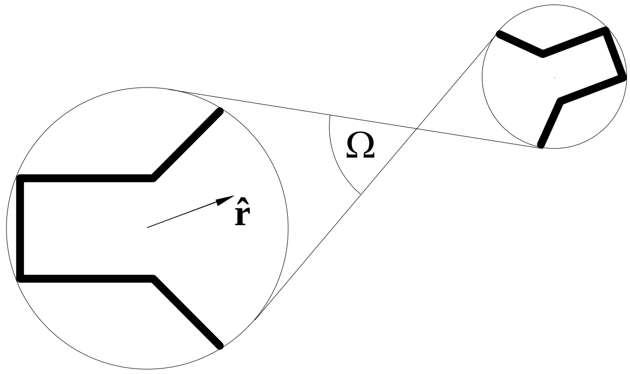

FIG. 1. *The sheaf of angles.*

As the separation between test antenna and probe increases (and Ω decreases), differences between distributed and local errors disappear (since $\|\mathbf{f}\|_{\Omega(\mathbf{r})} \to \|\mathbf{f}(\mathbf{r})\|$) and (5) reduces to a direction-by-direction far-field uncertainty formula with

$$\alpha \underset{r\to\infty}{\sim} \frac{r/\lambda}{\|\mathbf{s}(\hat{\mathbf{z}})\|}, \quad \beta \underset{r\to\infty}{\sim} \frac{1}{\|\mathbf{s}(\hat{\mathbf{z}})\|}. \tag{12}$$

In the standard far-field uncertainty analysis

$$\tau^2 = 1 + \sqrt{1 - |\mathbf{t}(\mathbf{r}) \cdot \mathbf{t}(\mathbf{r})| / \|\mathbf{t}(\mathbf{r})\|^2}. \tag{13}$$

The value $\tau^2 = 2$, which corresponds to a circularly polarized test antenna, yields a worst-case bound that depends only on the magnitude (and not the polarization) of $\mathbf{t}(\hat{\mathbf{r}})$.

4. Example.
Parameters α, β_1, and β_2, defined in (9)–(11), can be calculated readily from available information. Using (5), the uncertainty $u_t(\hat{\mathbf{r}})$ in the test antenna transmitting function can then be computed from the bounds $u_w(\mathbf{r})$ for the near-field measurement error and $u_s(\hat{\mathbf{z}})$ for the probe pattern error. Figure 2 shows examples of such calculations. In this figure, we use an AUT with mode limit $N = 50$ and a directivity of 30 dB (based on measurements of a Ku-band dish). The probe is a simulated maximum-directivity antenna with mode limit $N_P = 3$ and a directivity of 12 dB. The far-field separation is about $kr = 4N^2/\pi = 3200$. It is interesting that the far-field formulas (12) give good estimates for α and β throughout much of the radiating near-field region.

5. Estimating Multiple-Reflection Uncertainty.
Multiple reflections between the probe and test antenna have long been recognized as an important source of errors in near-field measurements [1], [5]. The separation between the probe and test antenna will change by $\lambda/4$ in going from a maximum (where the direct and first-order reflected signals add in phase) to a minimum (where they add out of phase). A simple method for estimating uncertainties due to multiple reflections between the test antenna and probe in near-field spherical-scanning measurements was described in [10]. To estimate uncertainties in far-field parameters, we measure the test antenna by scanning the probe over two spheres whose radii differ by a quarter wavelength ($\lambda/4$).

To test our idea, we measured a 60 cm diameter Cassegrain dish at 16 GHz over two concentric spheres—the first with a measurement radius of 151.5 cm and the second with a measurement radius of $\lambda/4 \approx 0.5$ cm greater than the first. For the 151.5 cm measurement radius data, the antenna directivity was 36.13 dB. For the 152 cm measurement radius data, the directivity was 36.07 dB. Without multiple reflections, the uncertainty in the directivity is ± 0.02 dB and is due primarily to drift and noise. Figure 3 shows cuts of the co-polarization and cross-polarization far-field patterns, respectively. We also determined the RMS value of the differences for the entire pattern. Relative to the pattern peak, these are

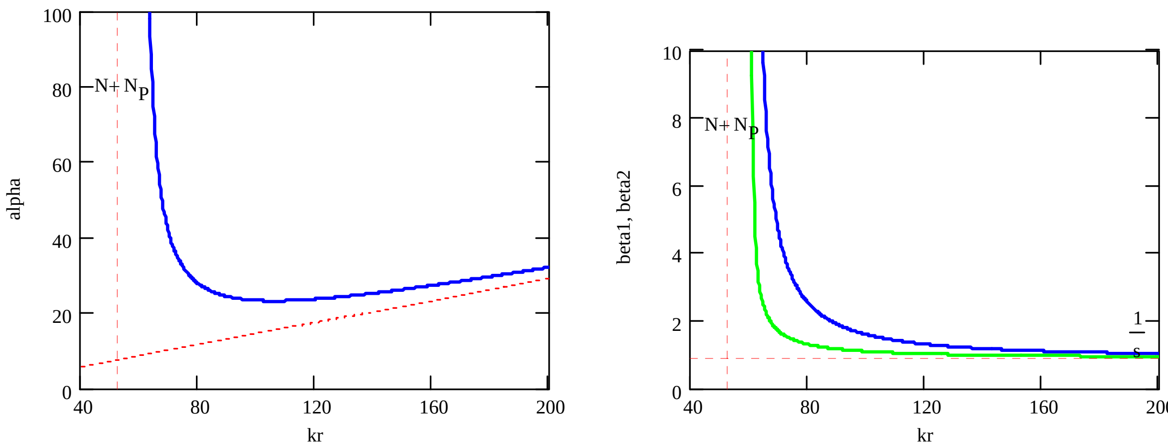

a. α versus kr b. β_1 and β_2 versus kr ($\beta_1 \le \beta_2$)

FIG. 2. *The vertical dashed lines indicate the approximate contact separation $kr = N + N_P$. The remaining dashed lines are the far-field asymptotes (12)*

θ component:	-59 dB
ϕ component:	-54 dB
Total pattern:	-53 dB.

This method is similar to one currently employed at NIST in estimating multiple-reflection effects in planar-near-field measurements.

6. Conclusion.

We have laid a foundation for future development of an uncertainty analysis for spherical near-field scanning measurements. This analysis divides neatly into terms due to uncertainties in the probe properties and to uncertainties in the near-field measurements. We expect the spherical near-field uncertainty analysis to approach the well-known far-field uncertainty analysis as the measurement radius increases. We have also presented a method for estimating uncertainties due to multiple reflections between the probe and test antenna.

REFERENCES

[1] J. E. Hansen, editor, *Spherical Near-field Antenna Measurements,* Chap. 6, Peter Peregrinus Ltd., 1988.

[2] A. C. Newell, G. Hindman, and C. F. Stubenrauch, "The Effect of Measurement Geometry on Alignment Errors in Spherical Near-Field Measurements," *Proc. Ant. Meas. Tech. Assoc.,* pp. 274–279, October 1999.

[3] A. C. Newell and G. Hindman, "The Alignment of a Spherical Near-Field Rotator Using Electrical Measurements," *Proc. Ant. Meas. Tech. Assoc.,* pp. 131–136, October 1997.

[4] D. W. Hess, "An Expanded Approach to Spherical Near-Field Uncertainty Analysis," *Proc. Ant. Meas. Tech. Assoc.,* pp. 495–500, October 2002.

[5] A. C. Newell, "Error Analysis Techniques for Planar Near-Field Measurements," *IEEE Trans. Antennas Propagat.,* vol. AP-36, no. 6, pp. 754–768, June 1988.

[6] A. C. Newell and D. Lee, "Application of the NIST 18 Term Error Model to Cylindrical Near-Field Antenna Measurements," *Proc. Ant. Meas. Tech. Assoc.,* pp. 24–29, October 2000.

[7] J. D. Jackson, *Classical Electrodynamics*, 2nd edition, Wiley, 1975

[8] R. C. Wittmann and M. H. Francis, "Spherical-Scanning Measurements: Propagating Errors Through the Near- to Far-Field Transformation," *Proc. Ant. Meas. Tech. Assoc.,* pp. 74–89, October 2004.

[9] A. D. Yaghjian, "Efficient Computation of Antenna Coupling and Fields Within the Near-Field Region," *IEEE Trans. Antennas Propagat.,* vol. AP-30, pp. 113–128, January 1982.

[10] M. H. Francis, J. R. Guerrieri, K. MacReynolds, and R. C. Wittmann, "Estimating Multiple-Reflection Uncertainties in Spherical Near-Field Measurements," *Proc. Ant. Meas. Tech. Assoc.,* pp. 85–88, October 2004.

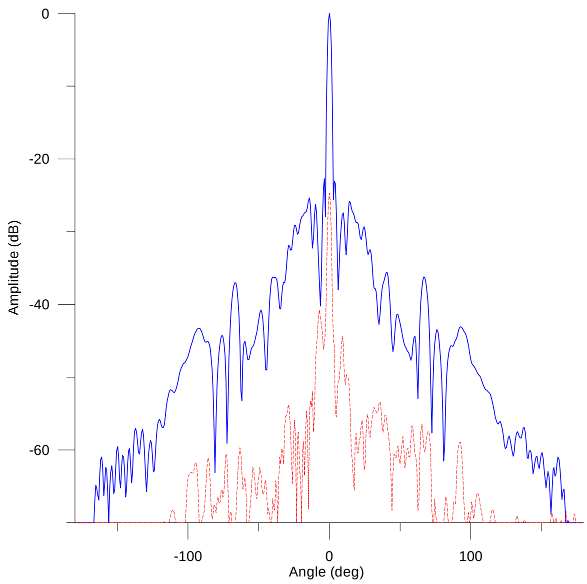

a. Co-polarization

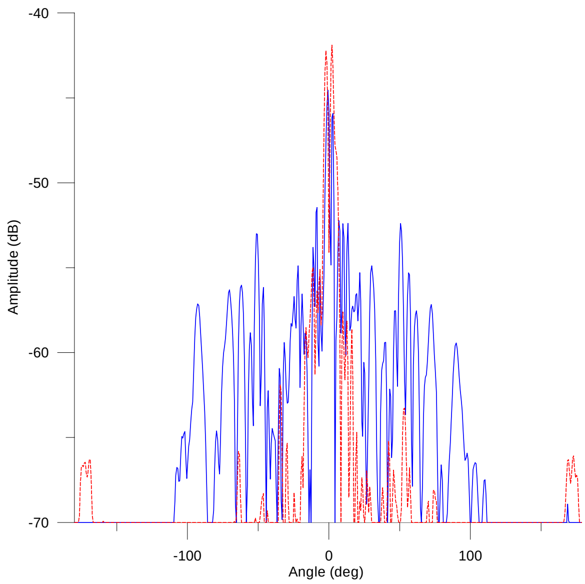

b. Cross-polarization

FIG. 3. *The $\phi = 90°$ cut of the far-field pattern from measurements at a radius of 151.5 cm (solid line) compared to the difference between the far-field patterns from measurements at 151.5 cm and 152 cm (dashed line).*